Acta Mech 198, 209–233 (2008)
DOI 10.1007/s00707-007-0528-7
Printed in The Netherlands

Acta Mechanica

Reformulation of Mindlin–Reissner governing equations of functionally graded circular plates

A. Nosier, F. Fallah

Department of Mechanical Engineering, Sharif University of Technology, Tehran, Iran

Received 30 June 2007; Accepted 11 October 2007; Published online 14 February 2008

Summary. The governing equations of the first-order shear deformation plate theory for FG circular plates are reformulated into those describing the interior and edge-zone problems. Analytical solutions are obtained for axisymmetric and asymmetric behavior of functionally graded circular plates with various clamped and simply-supported boundary conditions under mechanical and thermal loadings. The material properties are graded through the plate thickness according to a power–law distribution of the volume fraction of the constituents. The results, which are in closed form and suitable for design purposes, are verified with known results in the literature. It is shown that there are two boundary-layer equations. The effects of material property, plate thickness, boundary conditions, and boundary-layer phenomena on various response quantities in a solid circular plate are studied and discussed. Under a mechanical load, the responses of FG solid circular plates with various clamped supports are seen to be identical. It is observed that the boundary-layer width is approximately equal to the plate thickness with the boundary-layer effects in clamped FG plates being stronger than those in simply-supported plates. Also an exact solution is developed for the one-dimensional heat conduction equation with variable heat conductivity coefficient.

1 Introduction

Functionally graded materials (FGMs) are first introduced in 1984 by material scientists in Japan as thermal barrier materials [1] in a high temperature environment. They belong to a new class of materials which are microscopically heterogeneous and their material properties vary continuously. This is achieved by gradually changing the volume fraction of the constituent materials along a certain dimension (usually in the thickness direction). Due to the smooth variation of material properties, they offer many advantages over laminated composite materials including improved fatigue resistance, reduction of thermal stresses, residual stresses and interlaminar stresses, and more efficient joining techniques. Thus, FGMs are finding applications in many fields such as aerospace, power generation industries, and energy conversion. Sureh and Mortensen [2] provide an excellent introduction to the fundamentals of FGMs.

Circular plates made of FGMs are often employed as a part of engineering structures. Studies on FG circular plates are, however, rare. Durodola and Attia [3] investigated the deformation and stresses in

Correspondence: Asghar Nosier, Department of Mechanical Engineering, Sharif University of Technology, P.O. Box 11365-9567, Azadi Ave., Tehran, Iran
e-mail: nosier@sharif.edu

fiber-reinforced functionally graded rotating disks. They used the finite element method and direct numerical integration to solve the governing differential equations. Kawamura et al. [4] considered the multipurpose optimization of material composition for a functionally graded circular plate within the classical plate theory. In their analysis, they studied the one-dimensional transient heat conduction and the axisymmetric thermal bending problem of a non-homogeneous circular plate. Several authors have investigated the buckling of functionally graded circular plates [5], [6]. Najafizadeh and Eslami [7], [8] studied the buckling of FG circular plates under uniform radial compression and different types of thermal loadings. Cheng and Batra [9] used the method of asymptotic expansion to study the three-dimensional thermoelastic deformations of a rigidly clamped functionally graded elliptic plate. Reddy et al. [10] studied the axisymmetric bending of functionally graded solid and annular circular plates using the first-order shear deformation plate theory (FSDT), in which the solutions are expressed in terms of those obtained within the classical plate theory. Ma and Wang [11] found the relationships between axisymmetric bending and buckling solutions of functionally graded circular plates based on the third-order shear deformation plate theory and the classical plate theory. Based on the classical nonlinear von Karman plate theory, axisymmetric bending and post-buckling of functionally graded circular plates subjected to mechanical and thermal loadings were studied by Ma and Wang [12]. From the review of literature it appears that although axisymmetric buckling and bending of FG circular plates have been taken up by some researchers, little work is available on asymmetric problems of circular plates. The authors have so far come across only one paper dealing with asymmetric vibration and stability of FG circular plates [13] and have not come across any paper dealing with asymmetric bending of FG circular plates.

Both displacement-based and stress-based FSDT theories for isotropic plates result in a system of three differential equations in terms of three variables with a total degree of six. The displacement-based theory was introduced by Mindlin [14] while the stress-based theory was introduced by Reissner [15]. Reissner [15], [16] was the first to determine that for a homogenous isotropic plate his sixth-order theory can be uncoupled into two equations: edge-zone and interior equations. Nosier and Reddy [17]–[20] studied edge-zone and interior equations of several shear deformation plate theories for symmetrically laminated composite plates with transversely isotropic layers. Nosier et al. [21], [22] have studied boundary-layer phenomena in symmetrically laminated circular plates with transversely isotropic layers. They showed that the bending equations of several refined linear theories of symmetric laminated plates, with transversely isotropic layers (which are three differential equations in terms of three variables with a total degree of six), can be uncoupled into two equations, one in terms of transverse displacement, w, and the other in terms of a potential function, Φ, called the boundary layer function [18]. They demonstrated that all displacement-based theories except Reddy's theory [23] can be uncoupled to form a fourth-order interior equation and a second-order edge-zone equation.

In the present study the linear pre-buckling equilibrium equations within FSDT describing the bending-extension problem of FG circular plates are reformulated into interior and edge-zone equations. Since in FG plates, as opposed to isotropic plates or symmetrically laminated plates, the condition of middle-plane symmetry no longer exists, the extension and bending equations are coupled so that the governing equations are five coupled differential equations in terms of five variables with a total order of ten. Here these equations are uncoupled into five equations, whose total order will be the same as that of the original equations; two second-order differential equations defining the edge-zone problem of the FG plate in terms of two potential functions Φ and ξ (called boundary-layer functions), a fourth-order equation in terms of the transverse deflection w, and two first-order equations in terms of in plane middle surface displacement components u and v. This uncoupling makes it possible to present an analytical solution for asymmetric bending of FG circular plates in the linear pre-buckling range. Different types of clamped and simply-supported boundary

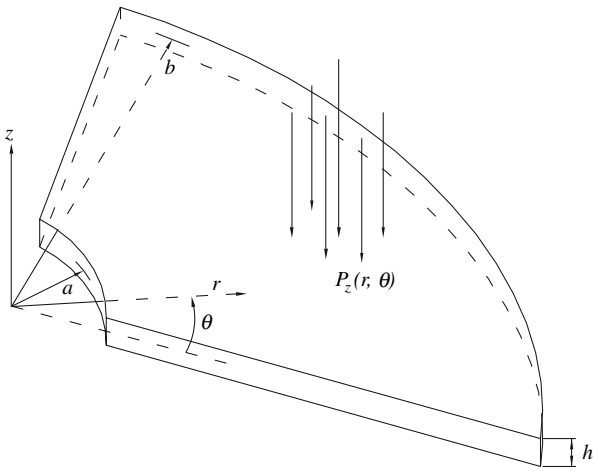

Fig. 1. Geometry of a FG circular plate and the coordinate system

conditions are considered. Under thermal and asymmetric mechanical loadings the effects of material properties, plate thickness, boundary conditions, and boundary-layer functions on deflections and stresses for a solid circular plate are studied and discussed in detail.

2 Theoretical formulation

A functionally graded circular plate of inner and outer radius of, respectively, a and b and thickness h is considered here. The geometry of the plate and the coordinate system is shown in Fig. 1. FGMs are modeled as a non-homogenous isotropic linear thermoelastic material whose properties, $\mathcal{P}$, vary continuously through the thickness of the plate, as a function of the volume fraction and properties of the constituent materials. Assuming the plate is made from a mixture of ceramic and metal, $\mathcal{P}$ can be expressed as [24]:

$$\mathcal{P} = \mathcal{P}_c \mathcal{V}_c + \mathcal{P}_m \mathcal{V}_m, \tag{1}$$

in which subscripts c and m refer to ceramic and metal, respectively. Also V_c and V_m are the volume fractions of ceramic and metal, respectively, which are related as follows:

$$V_c + V_m = 1. \tag{2}$$

The metal volume fraction is assumed to follow a power–law distribution as [10], [24]:

$$V_m = \left(\frac{h - 2z}{2h}\right)^n, \tag{3}$$

where n is the power–law index that takes values greater than or equal to zero. From Eqs. (1) through (3), the effective material property of an FG plate is, therefore, given by:

$$\mathcal{P}(z) = (\mathcal{P}_m - \mathcal{P}_c)\left(\frac{h - 2z}{2h}\right)^n + \mathcal{P}_c. \tag{4}$$

In the present study, relation (4) will be used as a model for the coefficient of thermal conductivity $\overline{K}$, the coefficient of thermal expansion α, and Young's modulus E of FG plates. The Poisson ratio υ is assumed to be a constant.

In thermal loading problems it is assumed that the temperature variation is only in the thickness direction. The one-dimensional heat conduction equation in the z-direction is given by:

$$-\frac{d}{dz}\left(\overline{K}(z)\frac{dT(z)}{dz}\right)=0 \tag{5}$$

with the boundary condition $T(h/2) = T_c$ and $T(-h/2) = T_m$. Here a stress-free state is assumed to exist at $T_0 = 0$°C. The thermal conductivity coefficient $\overline{K}(z)$ is assumed here to obey the power–law relation in (4). Separating the variables in Eq. (5) and substituting for $\overline{K}(z)$ yields:

$$dT = C_{1n}\frac{dz}{\Delta\overline{K}\left(\frac{1}{2}-\frac{z}{h}\right)^n+\overline{K}_c}, \tag{6}$$

where $\Delta\overline{K} = \overline{K}_m - \overline{K}_c$. Next, the following variables are introduced:

$$\frac{\overline{K}_c}{\Delta\overline{K}} = \beta^n \quad \text{and} \quad \frac{1}{2}-\frac{z}{h} = \lambda. \tag{7}$$

Substituting Eqs. (7) into (6) and integrating the result yields:

$$T(\lambda) = -C_{1n}\frac{h}{\Delta\overline{K}}\int\frac{d\lambda}{\lambda^n+\beta^n}+C_{2n}. \tag{8}$$

The exact solution for the integral appearing in (8) is given by Tuma in [25] for $n = 0.5$ and integer values of n. Using this exact solution in (8), the exact solution of Eq. (5) for $n = 0, 0.5$, and integer values of n may be presented as:

$$T(z) = -C_{1n}\frac{h}{\Delta\overline{K}}A_n(z)+C_{2n}, \tag{9.1}$$

where C_{1n} and C_{2n} are found by imposing the appropriate thermal boundary conditions on the top and bottom surfaces of the plate. The results are as follows:

$$C_{1n} = -\frac{(T_c-T_m)\Delta\overline{K}}{h[A_n(h/2)-A_n(-h/2)]},\ C_{2n} = \frac{T_mA_n(h/2)-T_cA_n(-h/2)}{[A_n(h/2)-A_n(-h/2)]} \quad n = 0, \frac{1}{2}, 1, 2, ... \tag{9.2}$$

with

$$A_0(z) = \frac{\Delta\overline{K}}{\overline{K}_m}\left(\frac{1}{2}-\frac{z}{h}\right),\quad A_{1/2}(z) = 2\sqrt{\frac{1}{2}-\frac{z}{h}}-2\frac{\overline{K}_c}{\Delta\overline{K}}\,\mathrm{Ln}\left(\sqrt{\frac{1}{2}-\frac{z}{h}}+\frac{\overline{K}_c}{\Delta\overline{K}}\right). \tag{10.1}$$

Also for the integer values of n the quantity A_n appearing in (9.1) is given by:

$$A_n(z) = \frac{2}{n\left(\frac{\overline{K}_c}{\Delta\overline{K}}\right)^{\frac{n-1}{n}}}\sum_{k=1}^{\frac{n-1}{2}}\sin\frac{2k\pi}{n}\tan^{-1}\left(\frac{\left(\frac{1}{2}-\frac{z}{h}\right)+\left(\frac{\overline{K}_c}{\Delta\overline{K}}\right)^{\frac{1}{n}}\cos\frac{2k\pi}{n}}{\left(\frac{\overline{K}_c}{\Delta\overline{K}}\right)^{\frac{1}{n}}\sin\frac{2k\pi}{n}}\right)+\frac{\mathrm{Ln}\left[\left(\frac{1}{2}-\frac{z}{h}\right)+\left(\frac{\overline{K}_c}{\Delta\overline{K}}\right)^{\frac{1}{n}}\right]}{n\left(\frac{\overline{K}_c}{\Delta\overline{K}}\right)^{\frac{n-1}{n}}}$$

$$+\frac{1}{n\left(\frac{\overline{K}_c}{\Delta\overline{K}}\right)^{\frac{n-1}{n}}}\sum_{k=1}^{\frac{n-1}{2}}\cos\frac{2k\pi}{n}\mathrm{Ln}\left[\left(\frac{1}{2}-\frac{z}{h}\right)^2+2\left(\frac{\overline{K}_c}{\Delta\overline{K}}\right)^{\frac{1}{n}}\left(\frac{1}{2}-\frac{z}{h}\right)\cos\frac{2k\pi}{n}+\left(\frac{\overline{K}_c}{\Delta\overline{K}}\right)^{\frac{2}{n}}\right],$$

$$n = 1, 3, \ldots \tag{10.2}$$

$$A_n(z)=\frac{2}{n\left(\frac{\overline{K}_c}{\Delta\overline{K}}\right)^{\frac{n-1}{n}}}\sum_{k=1}^{\frac{n}{2}}\sin\frac{(2k-1)\pi}{n}\tan^{-1}\left(\frac{\left(\frac{1}{2}-\frac{z}{h}\right)+\left(\frac{\overline{K}_c}{\Delta\overline{K}}\right)^{\frac{1}{n}}\cos\frac{(2k-1)\pi}{n}}{\left(\frac{\overline{K}_c}{\Delta\overline{K}}\right)^{\frac{1}{n}}\sin\frac{(2k-1)\pi}{n}}\right)$$
$$+\frac{1}{n\left(\frac{\overline{K}_c}{\Delta\overline{K}}\right)^{\frac{n-1}{n}}}\sum_{k=1}^{\frac{n}{2}}\cos\frac{(2k-1)\pi}{n}\mathrm{Ln}\left[\left(\frac{1}{2}-\frac{z}{h}\right)^2+2\left(\frac{\overline{K}_c}{\Delta\overline{K}}\right)^{\frac{1}{n}}\left(\frac{1}{2}-\frac{z}{h}\right)\cos\frac{(2k-1)\pi}{n}+\left(\frac{\overline{K}_c}{\Delta\overline{K}}\right)^{\frac{2}{n}}\right],$$
$$n=2,4,6,... \tag{10.3}$$

2.1 Equilibrium equations

Within the first-order shear deformation plate theory, the displacement field in polar coordinates is given by [27]:

$$\begin{aligned}&u_1(r,\theta,z)=u(r,\theta)+z\Psi_r(r,\theta),\\&u_2(r,\theta,z)=v(r,\theta)+z\Psi_\theta(r,\theta),\\&u_3(r,\theta,z)=w(r,\theta),\end{aligned} \tag{11}$$

where u, v, and w denote the displacements of a point on the midplane of the plate along r, θ, and z coordinates, respectively, and Ψ_r and Ψ_θ represent the small rotations of a transverse normal about the θ- and r- axes, respectively. Upon substitution of Eq. (11) into the linear strain-displacement relations of elasticity [26] the strain components are obtained as follows:

$$\varepsilon_r=\varepsilon_1^0+zk_1,\quad \varepsilon_\theta=\varepsilon_2^0+zk_2,\quad \varepsilon_z=0,\quad \gamma_{\theta z}=k_4,\quad \gamma_{rz}=k_5,\quad \gamma_{r\theta}=\varepsilon_6^0+zk_6, \tag{12}$$

where

$$\begin{aligned}&\varepsilon_1^0=u_{,r},\quad \varepsilon_2^0=\frac{1}{r}(u+v_{,\theta}),\quad \varepsilon_6^0=\frac{1}{r}(u_{,\theta}-v)+v_{,r},\quad k_1=\Psi_{r,r},\quad k_2=\frac{1}{r}(\Psi_r+\Psi_{\theta,\theta})\\&k_6=\frac{1}{r}(\Psi_{r,\theta}-\Psi_\theta)+\Psi_{\theta,r},\quad k_4=\Psi_\theta+\frac{1}{r}w_{,\theta},\quad k_5=\Psi_r+w_{,r}.\end{aligned} \tag{13}$$

In Eq. (13) and what follows a comma followed by a coordinate variable indicates partial differentiation with respect to that variable.

Based on relations (12) and (13), by using the principle of minimum total potential energy [26] the equilibrium equations are readily found to be:

$$\begin{aligned}&\delta u\quad N_{r,r}+\frac{1}{r}(N_r-N_\theta)+\frac{1}{r}N_{r\theta,\theta}=0,\\&\delta v\quad N_{r\theta,r}+\frac{1}{r}N_{\theta,\theta}+\frac{2}{r}N_{r\theta}=0,\\&\delta\Psi_r\quad M_{r,r}+\frac{1}{r}(M_r-M_\theta)+\frac{1}{r}M_{r\theta,\theta}-Q_r=0,\\&\delta\Psi_\theta\quad M_{r\theta,r}+\frac{1}{r}M_{\theta,\theta}+\frac{2}{r}M_{r\theta}-Q_\theta=0,\\&\delta w\quad rQ_{r,r}+Q_{\theta,\theta}+Q_r=rP_z(r,\theta),\end{aligned} \tag{14}$$

where $P_z(r, \theta)$ is the pressure applied on the top surface of the plate (see Fig. 1) and the stress and moment resultants are defined as follows:

$$(N_r, N_\theta, N_{r\theta}) = \int_{-h/2}^{h/2} (\sigma_r, \sigma_\theta, \sigma_{r\theta}) dz, \quad (Q_\theta, Q_r) = \int_{-h/2}^{h/2} (\sigma_{\theta z}, \sigma_{rz}) dz,$$
$$(M_r, M_\theta, M_{r\theta}) = \int_{-h/2}^{h/2} (\sigma_r, \sigma_\theta, \sigma_{r\theta}) z dz. \tag{15}$$

The boundary conditions corresponding to Eq. (14) require the specification of (see Fig. 1) the following:

$$\left.\begin{array}{llll} \text{either} & u & \text{or} & N_r \\ \text{either} & v & \text{or} & N_{r\theta} \\ \text{either} & \Psi_r & \text{or} & M_r \\ \text{either} & \Psi_\theta & \text{or} & M_{r\theta} \\ \text{either} & w & \text{or} & Q_r \end{array}\right\} \text{at } r = \text{constant and} \quad \left.\begin{array}{llll} \text{either} & u & \text{or} & N_{r\theta} \\ \text{either} & v & \text{or} & N_\theta \\ \text{either} & \Psi_r & \text{or} & M_{r\theta} \\ \text{either} & \Psi_\theta & \text{or} & M_\theta \\ \text{either} & w & \text{or} & Q_\theta \end{array}\right\} \text{at } \theta = \text{constant}. \tag{16}$$

The linear thermoelastic constitutive relations of an isotropic material are given by [27]:

$$\left\{\begin{array}{c}\sigma_r \\ \sigma_\theta \\ \sigma_{r\theta}\end{array}\right\} = \frac{E}{1-\upsilon^2}\begin{bmatrix} 1 & \upsilon & 0 \\ \upsilon & 1 & 0 \\ 0 & 0 & \frac{1-\upsilon}{2} \end{bmatrix}\left(\left\{\begin{array}{c}\varepsilon_r \\ \varepsilon_\theta \\ \gamma_{r\theta}\end{array}\right\} - \left\{\begin{array}{c}1 \\ 1 \\ 0\end{array}\right\}\alpha\Delta T\right), \quad \left\{\begin{array}{c}\sigma_{\theta z} \\ \sigma_{rz}\end{array}\right\} = K^2\frac{E}{2(1+\upsilon)}\begin{bmatrix} 1 & 0 \\ 0 & 1 \end{bmatrix}\left\{\begin{array}{c}\gamma_{\theta z} \\ \gamma_{rz}\end{array}\right\}, \tag{17}$$

where ΔT is the temperature change relative to the stress-free state, υ is the Poisson ratio which is assumed to be constant through the thickness of the plate, and K^2 is a shear correction factor which is introduced in FSDT in order to improve the transverse shear rigidities of the plate (see, e.g., [27]). Also E and α are, respectively, Young's modulus and the coefficient of thermal expansion which are, on the other hand, assumed to vary according to the power law in (4). Upon substitution of Eqs. (12) into (17) and the subsequent results into Eqs. (15), the stress and moment resultants are obtained to be:

$$\begin{aligned}
&N_r = A_1\varepsilon_1^0 + (A_1 - 2A_2)\varepsilon_2^0 + B_1 k_1 + (B_1 - 2B_2)k_2 - N^T, \\
&N_\theta = (A_1 - 2A_2)\varepsilon_1^0 + A_1\varepsilon_2^0 + (B_1 - 2B_2)k_1 + B_1 k_2 - N^T, \quad N_{r\theta} = A_2\varepsilon_6^0 + B_2 k_6, \\
&M_r = B_1\varepsilon_1^0 + (B_1 - 2B_2)\varepsilon_2^0 + D_1 k_1 + (D_1 - 2D_2)k_2 - M^T, \\
&M_\theta = (B_1 - 2B_2)\varepsilon_1^0 + B_1\varepsilon_2^0 + (D_1 - 2D_2)k_1 + D_1 k_2 - M^T, \quad M_{r\theta} = B_2\varepsilon_6^0 + D_2 k_6, \\
&Q_\theta = K^2 A_2 k_4, \quad Q_r = K^2 A_2 k_5,
\end{aligned} \tag{18}$$

with the stiffness coefficients being defined as:

$$(A_1, B_1, D_1) = \int_{-h/2}^{h/2} \frac{E(z)}{1-\upsilon^2}(1, z, z^2) dz \quad \text{and} \quad (A_2, B_2, D_2) = \int_{-h/2}^{h/2} \frac{E(z)}{2(1+\upsilon)}(1, z, z^2) dz. \tag{19.1}$$

Also the thermal stress and moment resultants are given by:

$$(N^T, M^T) = \int_{-h/2}^{h/2} \frac{E(z)}{1-\upsilon}\alpha(z)T(z)(1, z) dz. \tag{19.2}$$

Using the power–law formula (4) in (19.1), the explicit expressions for the rigidities of FG plates are obtained and listed in Appendix B.

2.2 Displacement equilibrium equations

The displacement equilibrium equations may be obtained by substitution of Eqs. (13) and (18) into the force equilibrium equations appearing in (14). Assuming that the temperature variation in the plate is only in its thickness direction, the results are:

$$\delta u; \quad A_1\left[\frac{1}{r}(ru)_{,r}\right]_{,r} + A_2\frac{1}{r^2}u_{,\theta\theta} + (A_1 - A_2)\frac{1}{r}v_{,r\theta} - (A_1 + A_2)\frac{1}{r^2}v_{,\theta} + B_1\left[\frac{1}{r}(r\Psi_r)_{,r}\right]_{,r} + B_2\frac{1}{r^2}\Psi_{r,\theta\theta} + (B_1 - B_2)\frac{1}{r}\Psi_{\theta,r\theta} - (B_1 + B_2)\frac{1}{r^2}\Psi_{\theta,\theta} = 0; \tag{20.1}$$

$$\delta v; \quad (A_1 - A_2)\frac{1}{r}u_{,r\theta} + (A_1 + A_2)\frac{1}{r^2}u_{,\theta} + A_2\left[\frac{1}{r}(rv)_{,r}\right]_{,r} + A_1\frac{1}{r^2}v_{,\theta\theta} + (B_1 - B_2)\frac{1}{r}\Psi_{r,r\theta} + (B_1 + B_2)\frac{1}{r^2}\Psi_{r,\theta} + B_2\left[\frac{1}{r}(r\Psi_\theta)_{,r}\right]_{,r} + B_1\frac{1}{r^2}\Psi_{\theta,\theta\theta} = 0; \tag{20.2}$$

$$\delta\Psi_r; \quad B_1\left[\frac{1}{r}(ru)_{,r}\right]_{,r} + B_2\frac{1}{r^2}u_{,\theta\theta} + (B_1 - B_2)\frac{1}{r}v_{,r\theta} - (B_1 + B_2)\frac{1}{r^2}v_{,\theta} + D_1\left[\frac{1}{r}(r\Psi_r)_{,r}\right]_{,r} + D_2\frac{1}{r^2}\Psi_{r,\theta\theta} + (D_1 - D_2)\frac{1}{r}\Psi_{\theta,r\theta} - (D_1 + D_2)\frac{1}{r^2}\Psi_{\theta,\theta} - K^2A_2(\Psi_r + w_{,r}) = 0; \tag{20.3}$$

$$\delta\Psi_\theta; \quad (B_1 - B_2)\frac{1}{r}u_{,r\theta} + (B_1 + B_2)\frac{1}{r^2}u_{,\theta} + B_2\left[\frac{1}{r}(rv)_{,r}\right]_{,r} + B_1\frac{1}{r^2}v_{,\theta\theta} + (D_1 - D_2)\frac{1}{r}\Psi_{r,r\theta} + (D_1 + D_2)\frac{1}{r^2}\Psi_{r,\theta} + D_2\left[\frac{1}{r}(r\Psi_\theta)_{,r}\right]_{,r} + D_1\frac{1}{r^2}\Psi_{\theta,\theta\theta} - K^2A_2(\Psi_\theta + \frac{1}{r}w_{,\theta}) = 0; \tag{20.4}$$

$$\delta w; \quad K^2A_2[(r\Psi_r)_{,r} + \Psi_{\theta,\theta}] + K^2A_2\left[(rw_{,r})_{,r} + \frac{1}{r}w_{,\theta\theta}\right] = rP_z(r,\theta). \tag{20.5}$$

The governing equations in (20.1–5) are five coupled partial differential equations in terms of u, v, Ψ_r, Ψ_θ, and w, with a total order of ten. In order to facilitate the solutions of these equations, they will be reformulated here to yield uncoupled equations. Towards this goal, the following new variables are introduced:

$$\xi(r,\theta) = \frac{1}{r}[u_{,\theta} - (rv)_{,r}], \tag{21.1}$$

$$\eta(r,\theta) = \frac{1}{r}[v_{,\theta} + (ru)_{,r}], \tag{21.2}$$

$$\Phi(r,\theta) = \frac{1}{r}[\Psi_{r,\theta} - (r\Psi_\theta)_{,r}], \tag{21.3}$$

where ξ and Φ are, as will be seen, the boundary-layer functions. It is to be noted that twice the rotation (i.e., $2\omega_z$) of any volume element within the plate about the z-axis (see Fig. 1) is given by $2\omega_z = \frac{1}{r}[u_{1,\theta} - (ru_2)_{,r}] = \xi + z\Phi$. That is, ξ signifies the rotation of volume elements at the middle surface of the plate whereas at any other point within the plate rotation is governed by both ξ and Φ as a linear function of z. As it will be seen, these rotation functions have boundary-layer characters in a sense that the response quantities of the plates are influenced by these functions only in regions near the edges of the plates.

Next, Eq. (20.1) is differentiated with respect to θ, Eq. (20.2) is multiplied by r and differentiated with respect to r, and finally the two results are subtracted from each other to yield:

$$A_2\nabla^2\xi + B_2\nabla^2\Phi = 0, \tag{22}$$

where ∇^2 is the two-dimensional Laplace operator. Equation (20.1) is then multiplied by r and differentiated with respect to r, Eq. (20.2) is differentiated with respect to θ, and the two results are finally added to yield:

$$A_1\nabla^2\eta + B_1\nabla^2\left[\frac{1}{r}\Psi_{\theta,\theta} + \frac{1}{r}(r\Psi_r)_{,r}\right] = 0. \tag{23}$$

Similarly, by carrying out the same operations on Eqs. (20.3) and (20.4) the following two equations will readily be obtained:

$$B_2\nabla^2\xi + D_2\nabla^2\Phi - K^2A_2\Phi = 0 \tag{24}$$

and

$$B_1\nabla^2\eta + D_1\nabla^2\left[\frac{1}{r}\Psi_{\theta,\theta} + \frac{1}{r}(r\Psi_r)_{,r}\right] - K^2A_2\left[\frac{1}{r}\Psi_{\theta,\theta} + \frac{1}{r}(r\Psi_r)_{,r}\right] - K^2A_2\nabla^2 w = 0. \tag{25}$$

Equations (22) and (24) may, for convenience, be replaced by the following two equations:

$$\nabla^2\Phi - \mu^2\Phi = 0 \tag{26.1}$$

and

$$\nabla^2\xi + \frac{B_2}{A_2}\nabla^2\Phi = 0, \tag{26.2}$$

where $\mu^2 = K^2\,A_2^2\,/(A_2\,D_2 - B_2^2)$. It is next noted that Eq. (20.5) may be rewritten as:

$$\frac{1}{r}\Psi_{\theta,\theta} + \frac{1}{r}(r\Psi_r)_{,r} = -\nabla^2 w + \frac{1}{K^2A_2}P_z. \tag{27}$$

Substitution of Eq. (27) into Eqs. (23) and (25) will yield two equations in terms of η and w, which may alternatively be rewritten as:

$$\nabla^2\nabla^2 w = -\frac{1}{D}P_z + \frac{1}{K^2A_2}\nabla^2 P_z \tag{28.1}$$

and

$$\nabla^2\eta = -\gamma P_z, \tag{28.2}$$

where $1/D = A_1/(A_1D_1 - B_1^2)$ and $\gamma = B_1/(A_1D_1 - B_1^2)$. Thus, the coupled governing equations in (20.1–5) are replaced by the more convenient set of equations in (26.1, 2) and (28.1, 2). Another important point to be made here is the appearance of the Laplace operator in Eqs. (26.1, 2) and (28.1, 2), which makes them to be coordinate-free equations. Also, another uncoupling procedure for the equilibrium equations may be to search for an appropriate plane through the thickness of the plate so that the stretching-bending coupling will disappear from the original set of equilibrium equations appearing in (14). For this latter approach the readers are referred to a paper by Irschik [28]. It is noted here that Eqs. (20.1) and (20.2) may be represented as:

$$\eta_{,r} = -\frac{A_2}{A_1}\frac{1}{r}\left(\xi + \frac{B_2}{A_2}\Phi\right)_{,\theta} + \frac{B_1}{A_1}(\nabla^2 w)_{,r} - \frac{B_1}{A_1K^2A_2}P_{z,r} \tag{29.1}$$

and

$$\eta_{,\theta} = \frac{A_2}{A_1} r \left(\xi + \frac{B_2}{A_2} \Phi \right)_{,r} + \frac{B_1}{A_1} (\nabla^2 w)_{,\theta} - \frac{B_1}{A_1 K^2 A_2} P_{z,\theta}. \tag{29.2}$$

Equations (26.1,2) and (28.1) will be solved to yield the response quantities Φ, ξ, and w. Afterwards, instead of solving Eq. (28.2), relations (29.1, 2) will be used to yield η. It is to be noted that Eqs.(26.1, 2) and (28.1) are known, respectively, as the edge-zone (or boundary-layer) equations and the interior equation of the plate (also see [18], [21], [22]).

Next, it is noted that Eqs. (20.3) and (20.4) may be rewritten as:

$$\Psi_r = -w_{,r} + \frac{1}{K^2 A_2} \frac{1}{r} (B_2 \xi + D_2 \Phi)_{,\theta} + \frac{B_1}{K^2 A_2} \eta_{,r} - \frac{D_1}{K^2 A_2} (\nabla^2 w)_{,r} + \frac{D_1}{(K^2 A_2)^2} P_{z,r} \tag{30.1}$$

and

$$\Psi_\theta = -\frac{1}{r} w_{,\theta} - \frac{1}{K^2 A_2} (B_2 \xi + D_2 \Phi)_{,r} + \frac{B_1}{K^2 A_2} \frac{1}{r} \eta_{,\theta} - \frac{D_1}{K^2 A_2} \frac{1}{r} (\nabla^2 w)_{,\theta} + \frac{D_1}{(K^2 A_2)^2} \frac{1}{r} P_{z,\theta}. \tag{30.2}$$

Relations (29.1, 2) may be used to eliminate $\eta_{,r}$ and $\eta_{,\theta}$ from Eqs. (30.1, 2). When this is done, the following relations, for determining Ψ_r and Ψ_θ, are obtained:

$$\Psi_r = -w_{,r} + \frac{A_1 B_2 - A_2 B_1}{A_1 K^2 A_2} \frac{1}{r} \xi_{,\theta} + \frac{A_1 D_2 - B_1 B_2}{A_1 K^2 A_2} \frac{1}{r} \Phi_{,\theta} - \frac{D}{K^2 A_2} (\nabla^2 w)_{,r} + \frac{D}{(K^2 A_2)^2} P_{z,r} \tag{31.1}$$

and

$$\Psi_\theta = -\frac{1}{r} w_{,\theta} - \frac{A_1 B_2 - A_2 B_1}{A_1 K^2 A_2} \xi_{,r} - \frac{A_1 D_2 - B_1 B_2}{A_1 K^2 A_2} \Phi_{,r} - \frac{D}{K^2 A_2} \frac{1}{r} (\nabla^2 w)_{,\theta} + \frac{D}{(K^2 A_2)^2} \frac{1}{r} P_{z,\theta}. \tag{31.2}$$

It is noted here that if the identity $A_1 B_2 - A_2 B_1 = 0$, which holds for any assumption arbitrarily made regarding the distribution of Young's modulus as in (4) with Poisson's ratio being constant through the thickness of the plate (the assumption made in present study), is used, then relations (31.1, 2) indicate that the boundary-layer function ξ has no effect on the rotation functions Ψ_r and Ψ_θ . Lastly, it is to be noted that the functions u and v will be found by using relations (21.1) and (21.2) which are two coupled first-order partial differential equations.

2.3 General solutions for a complete circular plate

Here the general solutions of the governing equations are obtained for a complete circular plate. For such a plate, the response quantities must be periodic in the θ direction. Thus, to begin with, the boundary-layer function Φ may be represented as:

$$\Phi(r, \theta) = \sum_{m=0}^{\infty} \Phi_m(r) \cos m\theta + \sum_{m=1}^{\infty} \tilde{\Phi}_m(r) \sin m\theta \tag{32}$$

with Φ_m and $\tilde{\Phi}_m$ being two unknown functions of r. Substitution of Eq. (32) into (26.1) yields two modified Bessel equations whose general solutions are given by (e.g., see [29]):

$$\begin{Bmatrix} \Phi_m(r) \\ \tilde{\Phi}_m(r) \end{Bmatrix} = \begin{Bmatrix} A_{1m} \\ \tilde{A}_{1m} \end{Bmatrix} I_m(\mu r) + \begin{Bmatrix} A_{2m} \\ \tilde{A}_{2m} \end{Bmatrix} \mathcal{K}_m(\mu r) \quad \begin{Bmatrix} m = 0, 1, 2, \dots \\ m = 1, 2, \dots \end{Bmatrix}, \tag{33}$$

where A_{1m}, $A_{2m}\tilde{A}_{1m}$, and $\tilde{A}_{2m}$ are the integration constants and I_m and $\mathcal{K}_m$ are the modified Bessel functions of the first and second kind, respectively. Next it is assumed that:

$$\xi(r,\theta)=\sum_{m=0}^{\infty}\xi_m(r)\cos m\theta+\sum_{m=1}^{\infty}\tilde{\xi}_m(r)\sin m\theta. \tag{34}$$

Substituting (34) and (32) into (26.2) and integrating the results yields:

$$\xi_0(r)=-\frac{B_2}{A_2}\Phi_0(r)+B_{10}+B_{20}\ln r \tag{35.1}$$

and

$$(\xi_m(r),\tilde{\xi}_m(r))=-\frac{B_2}{A_2}(\Phi_m(r),\tilde{\Phi}_m(r))+(B_{1m},\tilde{B}_{1m})r^m+(B_{2m},\tilde{B}_{2m})r^{-m}\quad m=1,\,2,\,\ldots \tag{35.2}$$

where B_{10}, B_{20}, B_{1m}, B_{2m}, $\tilde{B}_{1m}$, and $\tilde{B}_{2m}$ are the integration constants. In obtaining the results in (35.1, 2) use is made of the identity $f''+\ r^{-1}f'\ -\ m^2\ r^{-2}f\ \equiv\ r^{m-1}\ [\ r^{1-2m}\ (r^m f)'\ ]'$, $m\ =\ 0,\ 1,\ 2$,.., with a prime here and in what follows indicating total differentiation with respect to the variable r. The transverse displacement function w and pressure P_z may be represented as:

$$w(r,\theta)=\sum_{m=0}^{\infty}w_m(r)\cos m\theta+\sum_{m=1}^{\infty}\tilde{w}_m(r)\sin m\theta \tag{36.1}$$

and

$$P_z(r,\theta)=\sum_{m=0}^{\infty}P_m(r)\cos m\theta+\sum_{m=1}^{\infty}\tilde{P}_m(r)\sin m\theta, \tag{36.2}$$

where $(P_m(r),\tilde{P}_m(r)\,)=\frac{1}{\pi}\int_{-\pi}^{\pi}P_z(r,\theta)(\cos m\theta,\,\sin m\theta)d\theta$ (e.g., see [29]). Upon substitution of Eqs. (36.1) and (36.2) into Eq. (28.1), the following result is obtained:

$$r^{m-1}\frac{d}{dr}\left(r^{1-2m}\frac{d}{dr}\left\{r^{2m-1}\frac{d}{dr}\left[r^{1-2m}\frac{d}{dr}\{r^m(w_m,\tilde{w}_m)\}\right]\right\}\right)=-\frac{1}{D}(P_m,\tilde{P}_m)$$
$$+\frac{1}{K^2A_2}r^{m-1}\frac{d}{dr}\left\{r^{1-2m}\frac{d}{dr}\left[r^m(P_m,\tilde{P}_m)\right]\right\}. \tag{37}$$

Direct integration of (37) will yield:

$$w_0(r)=-\frac{1}{D}q_{10}(r)+\frac{1}{K^2A_2}q_{20}(r)+D_{10}+D_{20}r^2+D_{30}\ln r+D_{40}r^2\ln r, \tag{38.1}$$

$$(w_1,\tilde{w}_1)=-\frac{1}{D}(q_{11},\tilde{q}_{11})+\frac{1}{K^2A_2}(q_{21},\tilde{q}_{21})+(D_{11},\tilde{D}_{11})r+(D_{21},\tilde{D}_{21})r^3$$
$$+(D_{31},\tilde{D}_{31})r^{-1}+(D_{41},\tilde{D}_{41})r\ln r, \tag{38.2}$$

$$(w_m,\tilde{w}_m)=-\frac{1}{D}(q_{1m},\tilde{q}_{1m})+\frac{1}{K^2A_2}(q_{2m},\tilde{q}_{2m})+(D_{1m},\tilde{D}_{1m})r^m+(D_{2m},\tilde{D}_{2m})r^{m+2}$$
$$+(D_{3m},\tilde{D}_{3m})r^{-m}+(D_{4m},\tilde{D}_{4m})r^{-m+2}\quad m=2,3,\ldots, \tag{38.3}$$

where

$$(q_{1m},\tilde{q}_{1m})=\frac{1}{r^m}\int\frac{1}{r^{1-2m}}\int\frac{1}{r^{2m-1}}\int\frac{1}{r^{1-2m}}\int\frac{1}{r^{m-1}}(P_m,\tilde{P}_m)drdrdrdr \tag{38.4}$$

and

$$(q_{2m}, \tilde{q}_{2m}) = \frac{1}{r^m} \int \frac{1}{r^{1-2m}} \int \frac{1}{r^{m-1}} (P_m, \tilde{P}_m) dr dr. \tag{38.5}$$

Next, relations (29.1, 2) are used to obtain the function η. Towards this goal, η is represented as:

$$\eta(r, \theta) = \sum_{m=0}^{\infty} \eta_m(r) \cos m\theta + \sum_{m=1}^{\infty} \tilde{\eta}_m(r) \sin m\theta. \tag{39}$$

Substituting (32), (34), (36.1, 2), and (39) into (29.2) and (29.1) will result, respectively, in:

$$\eta_m = -\frac{A_2}{A_1}\frac{r}{m}(\tilde{\xi}'_m + \frac{B_2}{A_2}\tilde{\Phi}'_m) + \frac{B_1}{A_1}\left\{ r^{m-1}\frac{d}{dr}\left[r^{1-2m}\frac{d}{dr}(r^m w_m)\right] - \frac{P_m}{K^2 A_2}\right\} \quad m = 1, 2, \ldots \tag{40.1}$$

$$\tilde{\eta}_m = \frac{A_2}{A_1}\frac{r}{m}(\xi'_m + \frac{B_2}{A_2}\Phi'_m) + \frac{B_1}{A_1}\left\{ r^{m-1}\frac{d}{dr}\left[r^{1-2m}\frac{d}{dr}(r^m \tilde{w}_m)\right] - \frac{\tilde{P}_m}{K^2 A_2}\right\} \quad m = 1, 2, \ldots \tag{40.2}$$

and

$$\frac{d\eta_0}{dr} = \frac{B_1}{A_1}\frac{d}{dr}\left[\frac{1}{r}\frac{d}{dr}(r\frac{dw_0}{dr}) - \frac{P_0}{K^2 A_2}\right], \tag{41.1}$$

which upon direct integration yields:

$$\eta_0 = \frac{B_1}{A_1}\left[\frac{1}{r}\frac{d}{dr}(r\frac{dw_0}{dr}) - \frac{P_0}{K^2 A_2}\right] + H_{10}. \tag{41.2}$$

In Eq. (41.2) H_{10} is another integration constant. Next it is assumed that:

$$\left\{ \begin{array}{c} \Psi_r(r, \theta) \\ \Psi_\theta(r, \theta) \end{array} \right\} = \sum_{m=0}^{\infty} \left\{ \begin{array}{c} \Psi_{rm}(r) \\ \Psi_{\theta m}(r) \end{array} \right\} \cos m\theta + \sum_{m=1}^{\infty} \left\{ \begin{array}{c} \tilde{\Psi}_{rm}(r) \\ \tilde{\Psi}_{\theta m}(r) \end{array} \right\} \sin m\theta. \tag{42}$$

Substitution of Eqs. (42), (32), (34), and (36.1, 2) into (31.1, 2) will yield:

$$\begin{aligned} (\Psi_{rm}, \tilde{\Psi}_{rm}) = &-(w'_m, \tilde{w}'_m) + \frac{A_1 D_2 - B_1 B_2}{A_1 K^2 A_2}\frac{m}{r}(\tilde{\Phi}_m, -\Phi_m) + \frac{A_1 B_2 - A_2 B_1}{A_1 K^2 A_2}\frac{m}{r}(\tilde{\xi}_m, -\xi_m) \\ &- \frac{D}{K^2 A_2}\frac{d}{dr}\left(r^{m-1}\frac{d}{dr}\left\{ r^{1-2m}\frac{d}{dr}[r^m(w_m, \tilde{w}_m)]\right\}\right) + \frac{D}{(K^2 A_2)^2}(P'_m, \tilde{P}'_m), \end{aligned} \tag{43.1}$$

$$\begin{aligned} (\Psi_{\theta m}, \tilde{\Psi}_{\theta m}) = &-\frac{m}{r}(\tilde{w}_m, -w_m) - \frac{A_1 D_2 - B_1 B_2}{A_1 K^2 A_2}(\Phi'_m, \tilde{\Phi}'_m) - \frac{A_1 B_2 - A_2 B_1}{A_1 K^2 A_2}(\xi'_m, \tilde{\xi}'_m) \\ &- \frac{D}{K^2 A_2} m r^{m-2}\frac{d}{dr}\left\{ r^{1-2m}\frac{d}{dr}[r^m(\tilde{w}_m, -w_m)]\right\} + \frac{D}{(K^2 A_2)^2}\frac{m}{r}(\tilde{P}_m, -P_m). \end{aligned} \tag{43.2}$$

Finally, in order to determine the functions u and v, it is assumed that:

$$\left\{ \begin{array}{c} u(r, \theta) \\ v(r, \theta) \end{array} \right\} = \sum_{m=0}^{\infty} \left\{ \begin{array}{c} u_m(r) \\ v_m(r) \end{array} \right\} \cos m\theta + \sum_{m=1}^{\infty} \left\{ \begin{array}{c} \tilde{u}_m(r) \\ \tilde{v}_m(r) \end{array} \right\} \sin m\theta. \tag{44}$$

Substituting (34), (39), and (44) into (21.1) and (21.2) results in:

$$(r u_0)' = r\eta_0, \tag{45.1}$$

$$(r v_0)' = -r\xi_0, \tag{45.2}$$

$$m\tilde{u}_m - (r v_m)' = r\xi_m, \; -m v_m + (r\tilde{u}_m)' = r\tilde{\eta}_m \quad m = 1, 2, \ldots, \tag{45.3}$$

$$mu_m + (r\tilde{v}_m)' = -r\tilde{\xi}_m,\ m\tilde{v}_m + (ru_m)' = r\eta_m \quad m = 1, 2, \ldots \tag{45.4}$$

Equations (45.4) and (45.3) may alternatively be written as:

$$r^{m-1}\frac{d}{dr}\left[r^{1-2m}\frac{d}{dr}(r^{m+1}u_m)\right] = m\tilde{\xi}_m + \frac{1}{r}\frac{d}{dr}(r^2\eta_m) \quad m = 1, 2, \ldots, \tag{46.1}$$

$$\tilde{v}_m = \frac{r}{m}\eta_m - \frac{1}{m}(ru_m)' \quad m = 1, 2, \ldots \tag{46.2}$$

and

$$r^{m-1}\frac{d}{dr}\left[r^{1-2m}\frac{d}{dr}(r^{m+1}v_m)\right] = m\tilde{\eta}_m - \frac{1}{r}\frac{d}{dr}(r^2\xi_m) \quad m = 1, 2, \ldots, \tag{47.1}$$

$$\tilde{u}_m = \frac{r}{m}\xi_m + \frac{1}{m}(rv_m)' \quad m = 1, 2, \ldots \tag{47.2}$$

Integrating (45.1), (46.1), (45.2) and (47.1) yields:

$$u_0(r) = g_0(r) + E_{10}r^{-1}, \quad u_m(r) = g_m(r) + E_{1m}r^{m-1} + E_{2m}r^{-m-1} \quad m = 1, 2, \ldots \tag{48}$$

$$v_0(r) = \hbar_0(r) + F_{10}r^{-1}, \quad v_m(r) = \hbar_m(r) + F_{1m}r^{m-1} + F_{2m}r^{-m-1} \quad m = 1, 2, \ldots \tag{49}$$

where E_{10}, E_{1m}, E_{2m}, F_{10}, F_{1m}, and F_{2m} are the integration constants and

$$g_m(r) = \frac{1}{r^{m+1}}\int\frac{1}{r^{1-2m}}\int\frac{1}{r^{m-1}}\left[m\tilde{\xi}_m + \frac{1}{r}\frac{d}{dr}(r^2\eta_m)\right]drdr \quad m = 0, 1, 2, \ldots \tag{50}$$

$$\hbar_m(r) = \frac{1}{r^{m+1}}\int\frac{1}{r^{1-2m}}\int\frac{1}{r^{m-1}}\left[m\tilde{\eta}_m - \frac{1}{r}\frac{d}{dr}(r^2\xi_m)\right]drdr \quad m = 0, 1, 2, \ldots \tag{51}$$

Finally, substituting the second relations in (49) and (48) into (47.2) and (46.2), respectively, results in:

$$\tilde{u}_m = \frac{r}{m}\xi_m + \frac{1}{m}(r\hbar_m)' + F_{1m}r^{m-1} - F_{2m}r^{-m-1} \quad m = 1, 2, \ldots \tag{52}$$

$$\tilde{v}_m = \frac{r}{m}\eta_m - \frac{1}{m}(rg_m)' - E_{1m}r^{m-1} - E_{2m}r^{-m-1} \quad m = 1, 2, \ldots, \tag{53}$$

where ξ_m and η_m are given in (35.2) and (40.1), respectively. This completes the solution development for asymmetric thermo-mechanical bending of a functionally graded circular plate within the first-order shear deformation theory. It is to be mentioned here that in axisymmetric bending problems $v = \Psi_\theta = \frac{\partial}{\partial\theta} = 0$ and it can, therefore, be concluded from Eqs. (21.1) and (21.3) that $\xi\ (r) = \Phi\ (r) = 0$. That is, in axisymmetric problems there exists no boundary-layer effect.

2.4 Solid circular plate

In the present study, for numerical purposes, a functionally graded solid circular plate of radius b subjected to the following asymmetric transverse pressure (see Fig. 2) will be considered:

$$P_z(r, \theta) = \overline{P}_0 + \overline{P}_1\frac{r}{b}\cos\theta, \tag{54}$$

where $\overline{P}_0$ and $\overline{P}_1$ are two known parameters. By comparing Eq. (54) with (36.2) it is concluded that:

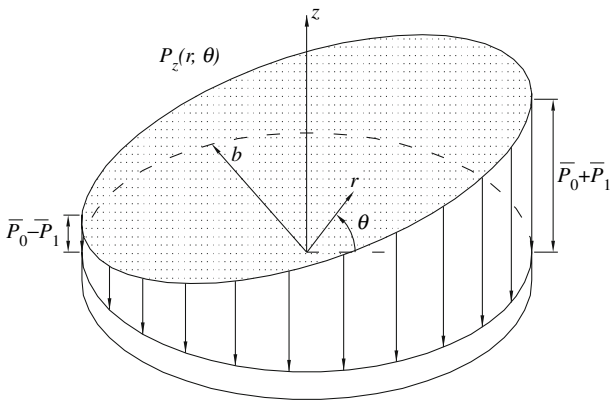

Fig. 2. FG solid circular plate subjected to an asymmetric pressure

$$P_0(r)=\overline{P}_0,\quad P_1(r)=\overline{P}_1\frac{r}{b}\quad\text{and}\quad P_m(r)=0,\quad m=2,3,\ldots,\tilde{P}_m(r)=0,\quad m=1,2,\ldots \tag{55}$$

Since all response quantities must be finite at $r=0$, for the pressure in (54) the response quantities of a solid circular plate are simplified to what follows (see the appropriate relations of the previous Section):

$$\begin{aligned}
&\Phi(r,\theta)=\tilde{\Phi}_1(r)\sin\theta,\quad \xi(r,\theta)=\tilde{\xi}_1(r)\sin\theta,\quad w(r,\theta)=w_0(r)+w_1(r)\cos\theta\\
&\eta(r,\theta)=\eta_0(r)+\eta_1(r)\cos\theta,\quad \Psi_r(r,\theta)=\Psi_{r0}(r)+\Psi_{r1}(r)\cos\theta,\quad \Psi_\theta(r,\theta)=\tilde{\Psi}_{\theta1}(r)\sin\theta\\
&u(r,\theta)=u_0(r)+u_1(r)\cos\theta,\quad v(r,\theta)=\tilde{v}_1(r)\sin\theta,
\end{aligned} \tag{56}$$

where

$$\begin{aligned}
&\tilde{\Phi}_1(r)=\tilde{A}_{11}I_1(\mu r),\quad \tilde{\xi}_1(r)=-\frac{B_2}{A_2}\tilde{A}_{11}I_1(\mu r)+\tilde{B}_{11}r\\
&w_0(r)=-\frac{\overline{P}_0r^4}{64D}+\frac{\overline{P}_0r^2}{4K^2A_2}+D_{10}+D_{20}r^2,\quad w_1(r)=-\frac{\overline{P}_1r^5}{192bD}+\frac{\overline{P}_1r^3}{8bK^2A_2}+D_{11}r+D_{21}r^3.
\end{aligned} \tag{57.1}$$

Furthermore, substitution of Eqs. (55) through (57.1) into Eqs. (41.1), (40.1, 2), (43.1,2), (48), and (53) will yield:

$$\begin{aligned}
&\eta_0(r)=-\gamma\frac{\overline{P}_0r^2}{4}+H_{10},\ \ \eta_1=-\gamma\frac{\overline{P}_1r^3}{8b}+\frac{8B_1D_{21}-A_2\tilde{B}_{11}}{A_1}r,\quad \Psi_{r0}=\frac{\overline{P}_0r^3}{16D}-2D_{20}r,\\
&\Psi_{r1}(r)=\frac{\tilde{A}_{11}}{\mu^2}\frac{I_1(\mu r)}{r}-\left(D_{11}+\frac{8D}{K^2A_2}D_{21}-\frac{A_1B_2-A_2B_1}{A_1K^2A_2}\tilde{B}_{11}\right)-3D_{21}r^2+\frac{5\overline{P}_1r^4}{192bD},\\
&\tilde{\Psi}_{\theta1}=-\frac{\tilde{A}_{11}}{\mu^2}\frac{d}{dr}[I_1(\mu r)]+\left(D_{11}+\frac{8D}{K^2A_2}D_{21}-\frac{A_1B_2-A_2B_1}{A_1K^2A_2}\tilde{B}_{11}\right)+D_{21}r^2-\frac{\overline{P}_1r^4}{192bD},\\
&u_0(r)=-\gamma\frac{\overline{P}_0r^3}{16}+H_{10}\frac{r}{2},\\
&u_1(r)=-\frac{B_2}{A_2}\frac{\tilde{A}_{11}}{\mu^2}\frac{I_1(\mu r)}{r}+\frac{A_1-3A_2}{8A_1}\tilde{B}_{11}r^2+\frac{3B_1}{A_1}D_{21}r^2-\frac{5\gamma\overline{P}_1r^4}{192b}+E_{11},\\
&\tilde{v}_1=\frac{B_2}{A_2}\frac{\tilde{A}_{11}}{\mu^2}\frac{d}{dr}[I_1(\mu r)]-\frac{3A_1-A_2}{8A_1}\tilde{B}_{11}r^2-\frac{B_1}{A_1}D_{21}r^2+\frac{\gamma\overline{P}_1r^4}{192b}-E_{11}.
\end{aligned} \tag{57.2}$$

It is to be noted that in Eqs. (57.1,2) there exist eight integration constants, namely, H_{10} ,D_{10}, D_{20},$\tilde{A}_{11}$, $\tilde{B}_{11}$,D_{11}, D_{21}, and E_{11}. The first three of these constants are, furthermore, realized to describe the axisymmetric bending of the FG circular plate. These eight constants are determined by imposing the appropriate boundary conditions at r = b. In order to study the edge effects on the response quantities, four types of clamped and four types of simply-supported boundary conditions are defined here, according to Eqs. (16), respectively, as follows:

$$C1: \Psi_r = \Psi_\theta = w = 0 \quad \text{and} \quad u = 0, v = 0, \tag{58.1}$$

$$C2: \Psi_r = \Psi_\theta = w = 0 \quad \text{and} \quad N_r = 0,\ v = 0, \tag{58.2}$$

$$C3: \Psi_r = \Psi_\theta = w = 0 \quad \text{and} \quad u = 0,\ N_{r\theta} = 0, \tag{58.3}$$

$$C4: \Psi_r = \Psi_\theta = w = 0 \quad \text{and} \quad N_r = 0,\ N_{r\theta} = 0 \tag{58.4}$$

and

$$S1: M_r = \Psi_\theta = w = 0 \quad \text{and} \quad u = 0,\ v = 0, \tag{59.1}$$

$$S2: M_r = \Psi_\theta = w = 0 \quad \text{and} \quad N_r = 0, \quad v = 0, \tag{59.2}$$

$$S3: M_r = \Psi_\theta = w = 0 \quad \text{and} \quad u = 0, \quad N_{r\theta} = 0, \tag{59.3}$$

$$S4: M_r = \Psi_\theta = w = 0 \quad \text{and} \quad N_r = 0, \quad N_{r\theta} = 0. \tag{59.4}$$

Imposing these boundary conditions at r = b yields two separate sets of algebraic equations which, upon solving, will yield, respectively, the constants H_{10}, D_{10}, and D_{20} and $\tilde{A}_{11}$, $\tilde{B}_{11}$,D_{11},D_{21}, and E_{11}. The results are, for convenience, presented in Appendix A. It is to be reminded here that in axisymmetric problems the boundary conditions in $C1$ and $C3$, $C2$ and $C4$, $S1$ and $S3$, and $S2$ and $S4$ will become identical since v and $N_{r\theta}$ are identically zero in such problems [see relations (18) and (13)].

3 Numerical results and discussions

To validate the results of the present study, results are obtained for isotropic plates and compared with the existing ones in the literature. By letting $K^2\ A_2 \to \infty$ in Eqs. (57.1), the relation for transverse deflection of an isotropic circular plate within the classical plate theory is obtained which is reported by Reddy in [27]. For an isotropic circular plate, on the other hand, the following is readily seen to hold (see Eqs. (19a)):

$$\begin{aligned} &A_1 = \frac{Eh}{1-\upsilon^2}; \quad A_2 = \frac{Eh}{2(1+\upsilon)}; \quad B_1 = B_2 = 0; \quad D_1 = \frac{Eh^3}{12(1-\upsilon^2)}; \quad D_2 = \frac{Eh^3}{24(1+\upsilon)}; \\ &D = \frac{A_1 D_1 - B_1^2}{A_1} = D_1. \end{aligned} \tag{60}$$

Upon Substitution of relations (60) into the appropriate relations of Appendix A (and letting $K^2\ A_2 \to \infty$), the following results are readily obtained:

$$\begin{aligned} &D_{10}(C) = -\frac{\overline{P}_0 b^4}{64D}, \quad D_{20}(C) = \frac{\overline{P}_0 b^2}{32D}, \quad D_{11}(C) = -\frac{\overline{P}_1 b^3}{192D}, \quad D_{21}(C) = \frac{\overline{P}_1 b}{96D}, \\ &D_{10}(S) = -\frac{5+\upsilon}{1+\upsilon}\frac{\overline{P}_0 b^4}{64D}, \quad D_{20}(S) = \frac{3+\upsilon}{1+\upsilon}\frac{\overline{P}_0 b^2}{32D}, \quad D_{11}(S) = -\frac{7+\upsilon}{3+\upsilon}\frac{\overline{P}_1 b^3}{192D}, \quad D_{21}(S) = \frac{5+\upsilon}{3+\upsilon}\frac{\overline{P}_1 b}{96D}. \end{aligned} \tag{61}$$

These results were previously obtained by Reddy in [27]. Furthermore, the numerical results for axisymmetric bending of an FG circular plate with various boundary conditions are obtained and

Table 1. Comparison of non-dimensional center deflections obtained within the present study with those presented by Reddy et al. [10] in axisymmetric bending of an FG circular plate under a uniform transverse pressure ($\upsilon = 0.288$, $E_m/E_c = 0.396$, and h/b = 0.2)

n	Reddy et al. [10]			Present study		
	Clamped plate	Simply-supported plate	Roller-supported plate	Clamped plate $C1$, $C2$, $C3$, $C4$	Simply-supported plate $S1$, $S3$	Roller-supported plate $S2$, $S4$
0	2.979	10.822	10.822	2.9792	10.8216	10.8216
2	1.613	5.708	5.925	1.6133	5.7083	5.9247
10	1.333	4.855	4.882	1.3330	4.8551	4.8819
10^5	1.180	4.285	4.285	1.1798	4.2854	4.2854

compared with those presented by Reddy et al. in [10]. The results for non-dimensional deflection $\overline{w} = 64wD_c/Pb^4$ (with $D_c = E_c\, h^3/12(1 - \nu^2)$ and P being a uniform pressure) at the center of the plate are shown in Table 1. Excellent agreements are seen to exist between the two results.

In the remaining of the present work Aluminum–Zirconia as a system of FGM will be considered for the purpose of numerical illustrations. The material properties (i.e., Young's moduli, Poisson's ratios, and coefficients of heat conduction and thermal expansion) of Aluminum and Zirconia are, respectively, assumed to be [12]:

$$E_m = 70\,\mathrm{GPa}, \quad \upsilon_m = 0.3, \quad \overline{K}_m = 204\,\mathrm{W/mK}, \quad \alpha_m = 23 \times 10^{-6}\,^{\circ}C \tag{62.1}$$

and

$$E_c = 151\,\mathrm{GPa}, \quad \upsilon_c = 0.3, \quad \overline{K}_c = 2.09\,\mathrm{W/mK}, \quad \alpha_c = 10 \times 10^{-6}\,^{\circ}C \tag{62.2}$$

In all calculations the shear correction factor is taken to be 5/6 (a value introduced by Reissner for isotropic plates). Also, unless mentioned otherwise, the thickness to radius ratio (i.e., h/b) of the plate and the power–law index n appearing in (4) are assumed to be 0.1 and 3, respectively, and the results will be presented for $\theta = \pi/4$.

3.1 Mechanical loading

Here, the asymmetric bending of an FG solid circular plate (see Fig. 2) under a linearly varying transverse mechanical load [see Eq. (54)] is considered. For convenience, the following non-dimensional parameters are introduced:

$$\begin{aligned} &\overline{w} = wE_ch^2/(\overline{p}_0b^3), \quad \overline{\sigma}_{ij} = \sigma_{ij}\,h^2/(\overline{p}_0b^2), \quad \overline{\Phi} = \Phi E_ch^2/(\overline{p}_0b), \quad \overline{\xi} = \xi\,E_ch^2/(\overline{p}_0b^2) \\ &\delta\,\overline{\sigma}_{ij} = 100[\overline{\sigma}_{ij} - \overline{\sigma}_{ij}(\Phi = 0 \quad \text{and/or} \quad \xi = 0)]/\overline{\sigma}_{ij}. \end{aligned} \tag{63}$$

It is to be noted that the quantity $\delta\overline{\sigma}_{\mathrm{ij}}$ is introduced to study the boundary-layer effect on the stress components, and by $\overline{\sigma}_{ij}(\Phi = 0\,\text{and/or}\,\xi = 0)$ it is meant that in calculating the stress components the function(s) Φ and/or ξ will be set to zero. Also, unless mentioned otherwise, in all the numerical results presented the value of $\overline{P}_1$ is taken to be equal to $\overline{P}_0$.

Figure 3a shows the profile of the plate after deformation for four types of clamped and simply-supported boundary conditions. It is observed that the deflections for the four types of clamped supports exactly coincide with each other. The remaining response quantities (i.e. u, v, Ψ_r, and Ψ_θ) for the clamped supports are seen to be exactly the same except for the values of u and v in $C4$ support which differ from those of $C1$, $C2$, and $C3$ supports in a constant rigid-body translation.

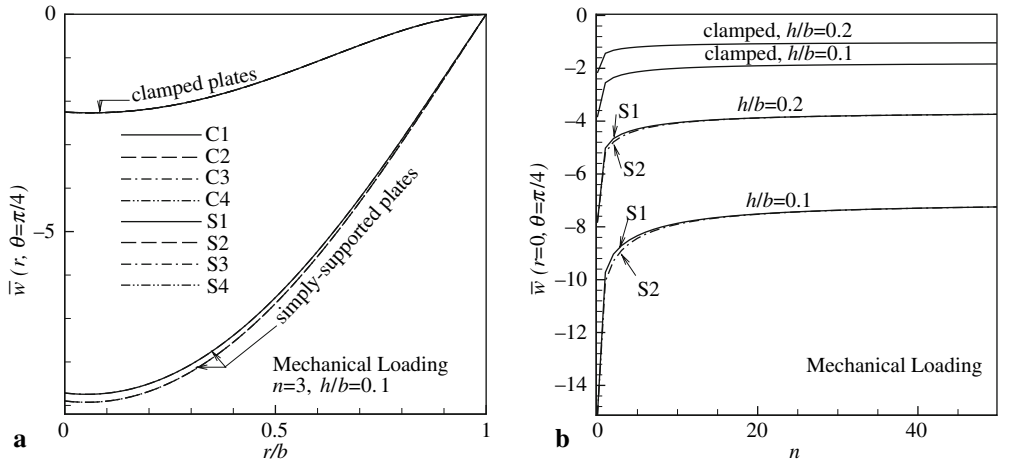

Fig. 3. **a** Transverse deflection of an FG solid circular plate with various boundary conditions and **b** center deflection of an FG solid circular plate with various edge supports as a function of power–law index n

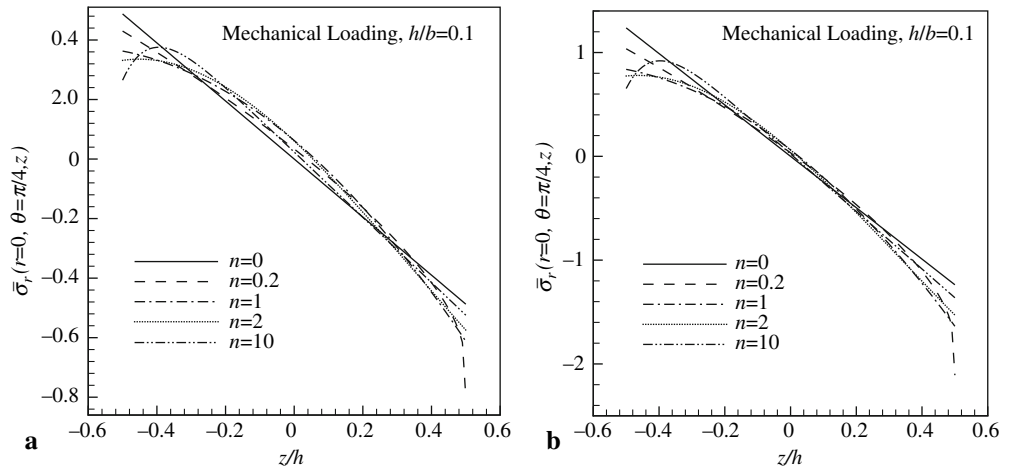

Fig. 4. Through-the-thickness radial stress distribution at the center of an FG solid circular plate with **a** clamped and **b** $S1$-type support as a function of power–law index n

This, on the other hand, is due to the fact that, in the absence of thermal loads, imposing $u = v = 0$ in $C1$ support [see Eqs. (58.1–4)] also yields the results $N_r = N_{r\theta} = 0$. Thus, imposing either $N_r = 0$ or $N_{r\theta} = 0$ or $N_r = N_{r\theta} = 0$ in the remaining three clamped supports will not cause any difference in the results. For this reason, when mechanical loading is considered, the four types of clamped supports are simply referred to as clamped (also see Table 1.). Also the results for $S3$ and $S4$ supports are very close to those of $S1$ and $S2$ supports, respectively. The effects of the power–law index n on the center deflection of clamped and various simply-supported plates are illustrated in Fig. 3b. It is seen that the metallic plate (i.e., $n = 0$) has the maximum deflection because of having the lowest stiffness and this deflection decreases significantly as n is increased from 0 to approximately 1 for a clamped plate and from 0 to approximately 3 for a simply-supported plate.

Figures 4a and b display the center radial stress distribution through the plate thickness for clamped and $S1$-type supported plates, respectively, under linearly varying loading (see Fig. 2) as a

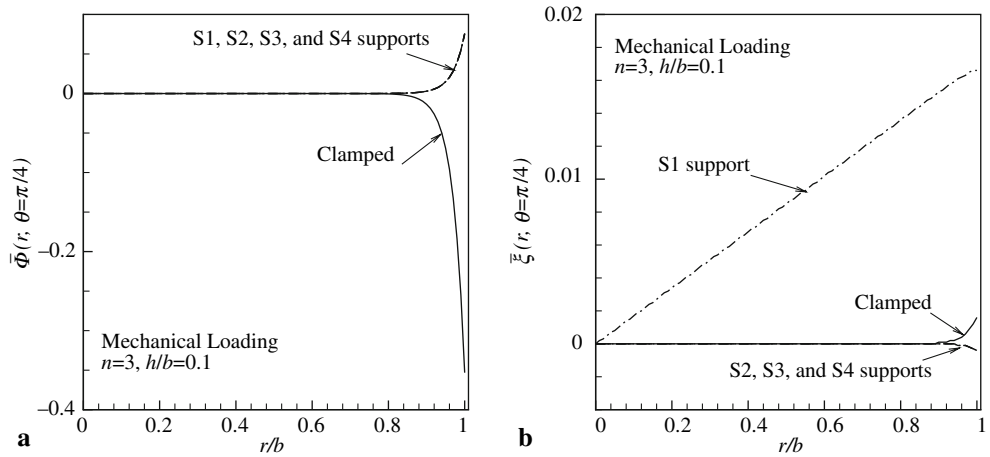

Fig. 5. Variations of boundary-layer functions **a** Φ and **b** ξ in FG solid circular plates with various edge supports

function of the power–law index n. For $n = 0$ the radial stress distribution is seen to be linear. For both boundary supports the stress at the top surface is compressive and its maximum occurs for $n = 0.2$. Also the radial stress at the bottom surface is tensile and its maximum occurs in a pure metallic plate (i.e. $n = 0$). At the center of the plate the hoop stress σ_θ is identical with the radial stress and the in-plane shear stress $\sigma_{r\theta}$ is zero for all values of n. At the other points of the plate the order of magnitudes of the radial and hoop stresses is the same while the order of magnitude of $\sigma_{r\theta}$ is less than that of radial stress. Since stresses in FG plates with $S2$-type support are very close to those of $S1$, the results for $S2$ support are not presented here. The stresses within the FG circular plates with $S3$-type and $S4$-type supports coincide with those of $S1$ and $S2$, respectively.

To study the boundary-layer phenomenon, plots of the boundary-layer functions Φ and ξ (as a function of r/b) for various support conditions are presented in Fig. 5a and b. Except for ξ in the $S1$ support, the functions Φ and ξ have a boundary-layer character. That is, except near the edges of the plate (i.e., in the edge-zone region), these functions are practically zero everywhere in the plate (i.e., in the interior region of the plate). It can be seen that the numerical values of Φ (and also ξ) in $S2$, $S3$, and $S4$ supports are exactly the same [see Eqs. (56), (57.1), (A.3a), and (A.3b)] and the numerical value of Φ in $S1$ is very close to those in $S2$, $S3$, and $S4$ supports. Also it is seen that the boundary-layer in a clamped FG circular plate is stronger than that in a simply-supported FG circular plate and, furthermore, the magnitude of Φ is considerably greater than ξ. The above observations can also be made in Figs. 6 and 7 in which the variations of boundary-layer functions Φ and ξ as functions of r and θ are displayed for clamped and $S2$-supported plates with $\overline{P}_1 = 2\overline{P}_0$. The variations of boundary-layer functions Φ and ξ as a function of h/b are presented in Fig. 8 for clamped plates. It is observed that the width of the boundary layer is approximately equal to the thickness of the plate. Furthermore, the magnitudes of Φ for various aspect ratios are seen to be approximately the same whereas that of ξ becomes larger as the thickness of the plate increases. The same results are seen to hold for simply-supported plates.

The effects of boundary-layer functions Φ and ξ on the transverse shear stress components, σ_{rz} and $\sigma_{\theta z}$, at $z = h/2$ are studied in Figs. 9 and 10. It is observed that the curves of $\delta\,\overline{\sigma}_{rz}$ and $\delta\overline{\sigma}_{\theta z}$ when $\Phi = \xi = 0$ and when $\Phi = 0$ alone exactly coincide with each other and the numerical values of $\delta\,\overline{\sigma}_{rz}$ and $\delta\,\overline{\sigma}_{\theta z}$ when $\xi = 0$ are zero everywhere. This indicates that the function ξ does not have any effect on the transverse shear stress components σ_{rz} and $\sigma_{\theta z}$. This, on the other hand, stems from the

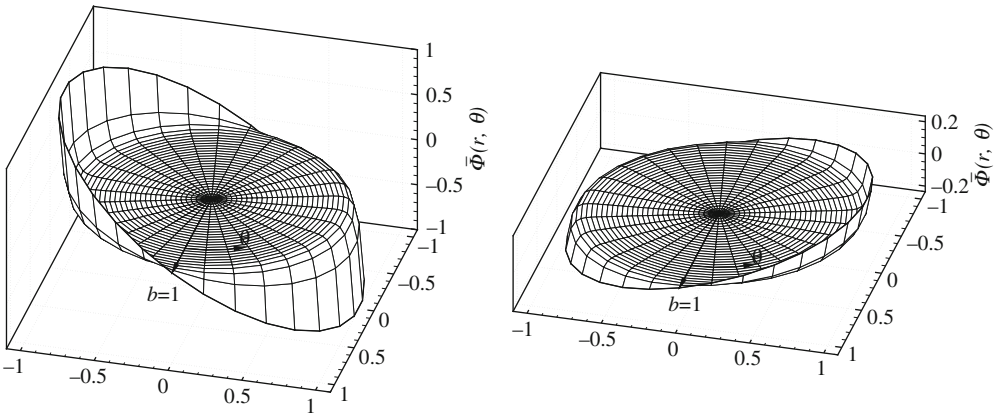

a Mechanical Loading, $\bar{P}_1$=2 $\bar{P}_0$, n =3, h/b=0.1 Clamped FG plate

b Mechanical Loading, $\bar{P}_1$=2 $\bar{P}_0$, n =3, h/b=0.1 S2-supported FG plate

Fig. 6. Variation of boundary-layer function Φ in an FG solid circular plate with **a** clamped and **b** $S2$-type support as a function of r and θ

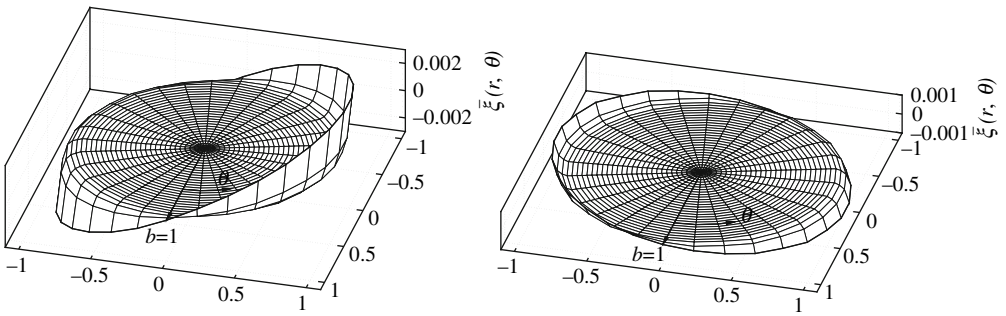

a Mechanical Loading, $\bar{P}_1$=2 $\bar{P}_0$, n=3, h/b=0.1 Clamped FG plate

b Mechanical Loading, $\bar{P}_1$=2 $\bar{P}_0$, n=3, h/b=0.1 S2-supported FG plate

Fig. 7. Variation of boundary-layer function ξ in an FG solid circular plate with **a** clamped and **b** $S2$-type support as a function of r and θ

fact that the rotation functions Ψ_r and Ψ_θ are not dependent on the function ξ, as it is discussed earlier [see Eqs. (31.1, 2)]. Also numerical results indicate that the curves of $\delta\,\overline{\sigma}_{rz}$ and $\delta\,\overline{\sigma}_{\theta z}$ for $S2$, $S3$, and $S4$ supports are the same as the ones presented for $S1$ support in Figs. 9 and 10. It is to be noted that the function Φ has a larger effect on $\sigma_{\theta z}$ than on σ_{rz} in both clamped and simply-supported FG circular plates.

3.2 Thermal loading

In thermal loading problems it is assumed that $T_m = 20°\text{C}$ and $T_c = 300°\text{C}$. The variations of temperature T at various planes within the plate as a function of n are displayed in Fig. 11. The minimum temperatures on planes at $z = -h/4$, $z = 0$, and $z = h/4$ are seen to occur when $n = 5$, $n = 3$ and $n = 2$, respectively, which may be taken into consideration in an optimization problem. It is to be reminded that for fractional values of n Eq. (5) is numerically integrated here. In the remaining of

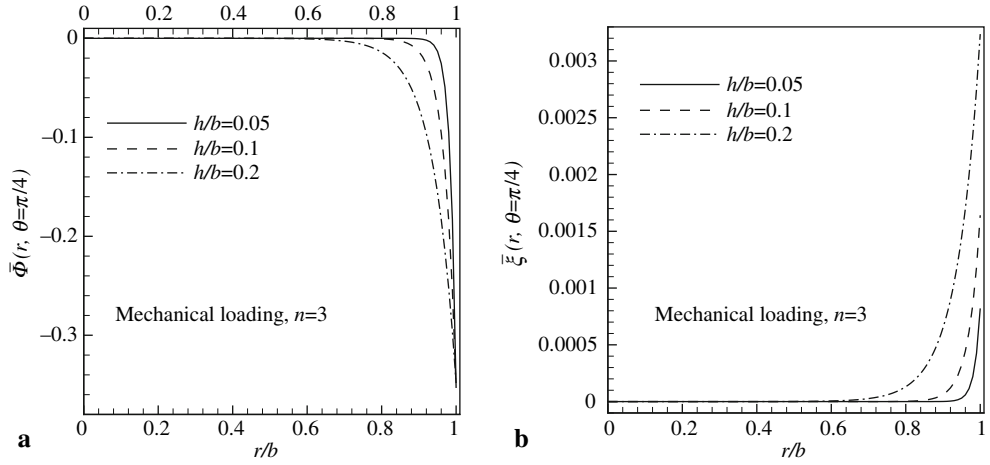

Fig. 8. Effect of thickness to radius ratio on boundary-layer functions **a** Φ and **b** ξ in a clamped FG solid circular plate

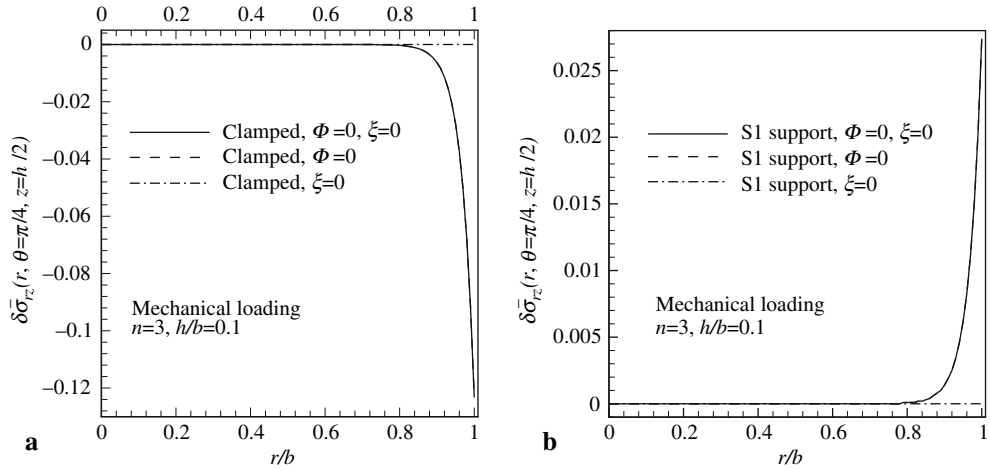

Fig. 9. Effects of boundary-layer functions on the transverse shear stress component σ_{rz} in **a** a clamped FG plate and **b** an $S1$-supported FG plate

the present study the following non-dimensional parameters for the transverse deflection w and the stress component σ_r will be employed:

$$\overline{w} = w/h, \quad \overline{\sigma}_r = 100\sigma_r h^2/(E_c \alpha_c T_c b^2). \tag{64}$$

Also in what follows, unless mentioned otherwise, it will be assumed that the power–law index n is equal to 3. It is to be noted that there will exist no boundary-layer effect [i.e., $\xi\,(r) = \Phi\,(r) = 0$] since the thermal problem considered here is an axisymmetric problem.

The transverse deflections of FG plates with different edge supports and aspect ratios (i.e., thickness to radius ratios) as functions of r are depicted in Fig. 12a. It is seen that bending does not occur in FG plates having any type of clamped supports (i.e., $C1$ through $C4$) as described in

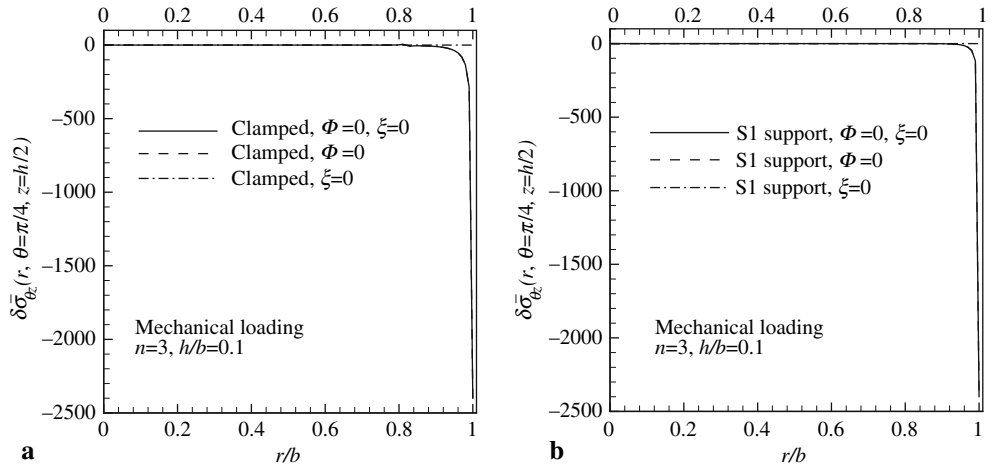

Fig. 10. Effects of boundary-layer functions on the transverse shear stress component $\sigma_{\theta z}$ in **a** a clamped FG plate and **b** an $S1$-supported FG plate

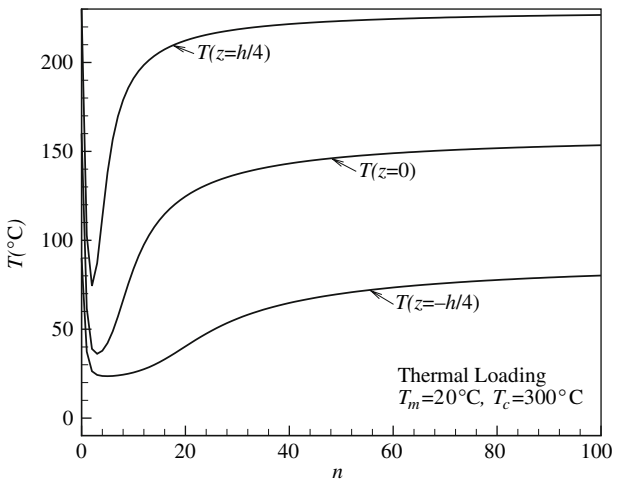

Fig. 11. Temperature variation on planes located at $z = -h/4$, $z = 0$, and $z = h/4$ as a function of power–law index n

(58.1–4). Also the deflections of plates with $S1$ and $S3$ edge supports are identical. The same conclusion is not only seen to hold for the deflections of FG plates with $S2$ and $S4$ supports but also for the remaining response quantities of the plates. Furthermore, it is to be noted that for simply-supported plates with smaller aspect ratios the deflections become considerably larger. The effects of the power–law index n on the transverse center deflections of FG plates with $S1$ and $S2$ supports are demonstrated in Fig. 12b. It is seen that similar to the trends of the temperature variation in Fig. 11 here the deflections of the plates are also significantly influenced by the numerical value of the power–law index n.

The center radial stress profiles of FG plates under thermal loading and with various boundary supports are shown in Fig. 13. It is seen that the radial stress σ_r is compressive through the thickness of the plate with $C1$ support. It is to be noted here that for plates under thermal loading the responses are no longer the same for various clamped supports. In fact, numerical results indicate that the responses are identical for plates with $C1$ and $C3$ supports. The same observation is made as far as $C2$ and $C4$ supports are concerned. This, on the other hand, is due to the fact that in thermal loading problems imposing the boundary conditions $u = v = 0$ will not make the resultant stress N_r vanish.

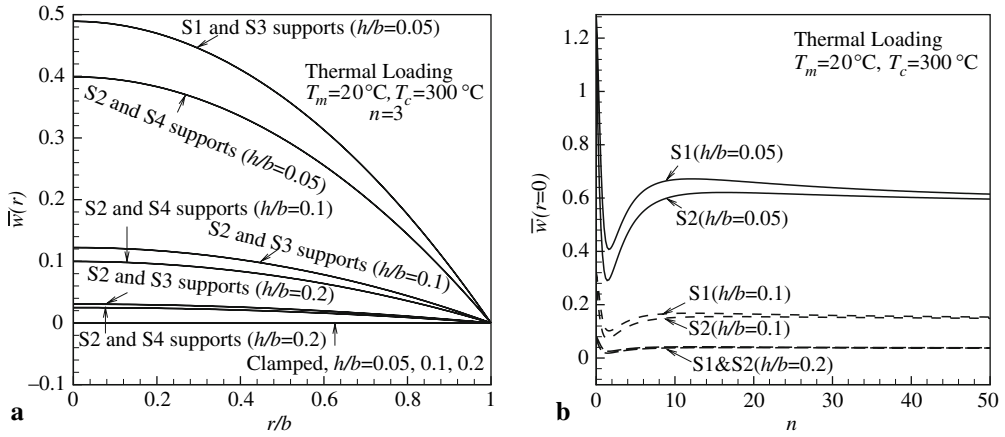

Fig. 12. **a** Transverse deflection of FG solid circular plates with various edge supports and **b** variation of transverse center deflection of an FG solid circular plate with various aspect ratios and edge supports as a function of n

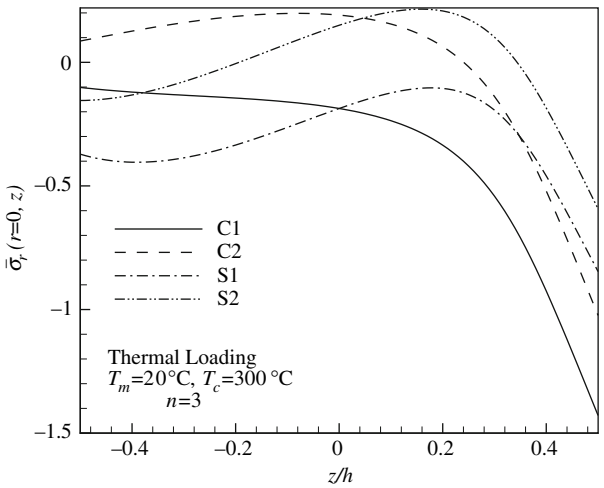

Fig. 13. Through-the-thickness distribution of radial stress at the center of FG plates with various edge supports

Finally, the variation of center radial stress σ_r at various planes in FG solid circular plates is displayed in Fig. 14 as a function of the power–law index n. It is observed that, similar to the temperature variation in Fig. 11, the radial stress reaches an extremum value as n increases regardless of the boundary support assumed for the FG plate.

4 Conclusions

In the present work, by introducing new variables, the appropriate equilibrium equations of FG plates within the first-order shear deformation theory are reformulated into interior and two boundary-layer equations. It is observed that the rotation of any volume element within the plate is governed by the two boundary-layer functions that are introduced in the present study. Analytical solutions are then developed for complete FG circular plates with various boundary conditions under an asymmetric mechanical load and a temperature variation through the plate thickness. The results

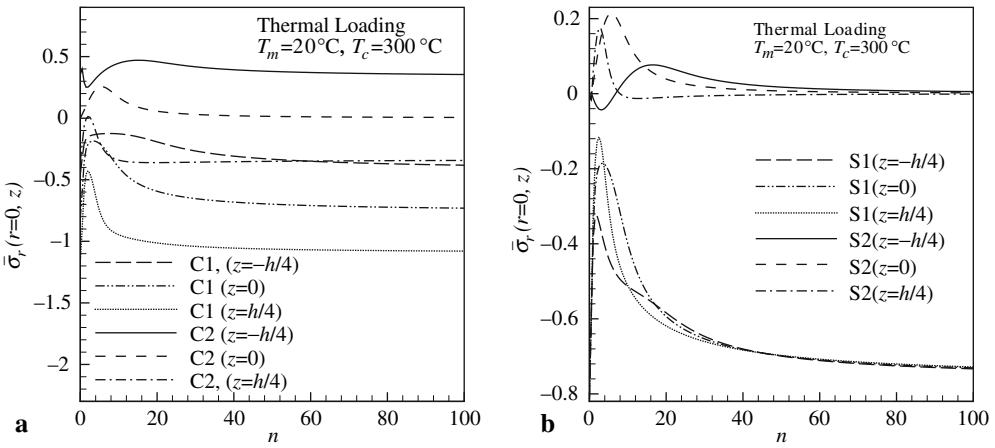

Fig. 14. Variation of center radial stress σ_r at various planes in FG circular plates with **a** clamped and **b** simply-supported edges as a function of n

for a solid circular plate are verified with known results in the literature. Several numerical results are generated to manifest the effects of the material constant (i.e., the power-index n), plate thickness, edge supports and boundary-layer functions on various response quantities. It is found that the boundary-layer width is approximately equal to the plate thickness. Furthermore, the boundary-layer effect in clamped FG plates is stronger than that in simply-supported plates and there exists no boundary-layer effect in axisymmetric problems. Also one of the boundary-layer functions is noted to affect only the in-plane stress components within the plates. Under a mechanical load, the responses of FG solid circular plates with various clamped supports are seen to be identical. Furthermore, for thermal loading, it is observed that bending does not occur in clamped FG plates.

An exact solution is presented for the one-dimensional heat conduction equation with variable heat conductivity coefficient. It is seen that the material constants have a significant influence on temperature distribution, deflection, and stress components within the FG plates.

Appendix A

For various clamped supports [see Eqs. (58.1–4)] the integration constants appearing in Eqs. (57.1, 2) are found to be as follows:

$$H_{10}(C1,C3)=\frac{\gamma\overline{P}_0 b^2}{8},\quad H_{10}(C2,C4)=\frac{\gamma\overline{P}_0 b^2}{8}+\frac{N^T}{A_1-A_2}, \tag{A.1.1}$$

$$D_{10}(C1,C2,C3,C4)=-\frac{\overline{P}_0 b^4}{64D}-\frac{\overline{P}_0 b^2}{4K^2A_2},\quad D_{20}(C1,C2,C3,C4)=\frac{\overline{P}_0 b^2}{32D}, \tag{A.1.2}$$

$$\begin{aligned}&\tilde{A}_{11}(C1,C2,C3,C4)=-\frac{\mu^2\overline{P}_1 b^4}{e_0},\quad \tilde{B}_{11}(C1,C2,C3,C4)=0,\\ &D_{11}(C1,C2,C3,C4)=-\overline{P}_1 b\frac{e_2[I_0(\mu b)+I_2(\mu b)]+e_3 I_1(\mu b)}{16K^2A_2De_0},\\ &D_{21}(C1,C2,C3,C4)=\overline{P}_1 b\frac{e_4[I_0(\mu b)+I_2(\mu b)]+e_5 I_1(\mu b)}{8De_0},\end{aligned} \tag{A.1.3}$$

$$E_{11}(C1,C2,C3)=\overline{P}_1 b^3\frac{e_6[I_0(\mu b)+I_2(\mu b)]+e_7 I_1(\mu b)}{16A_1 D e_0},\quad E_{11}(C4)=0, \tag{A.1.4}$$

where the constant D is first introduced in Eq. (28.1) and

$$\begin{aligned}
&e_0=12[e_1(I_0(\mu b)+I_2(\mu b))-8DI_1(\mu b)],\quad e_1=\mu b(4D+e_{01}),\\
&e_2=\mu b(96D^2+32e_{01}D+e_{01}^2),\quad e_3=-16D(12D+e_{01}),\quad e_4=\mu b(6D+e_{01}),\\
&e_5=-12D,\quad e_6=-\mu b B_1(16D+e_{01}),\quad e_7=16B_1D,\quad e_{01}=K^2A_2b^2.
\end{aligned} \tag{A.1.5}$$

For various simply-supported plates the constants H_{10}, D_{10}, and D_{20} are found to be:

$$H_{10}(S1,S3)=\frac{\gamma\overline{P}_0 b^2}{8},\quad H_{10}(S2,S4)=\frac{f_2M^T-f_3N^T+f_2f_4(\overline{P}_0b^2/8)}{f_0}, \tag{A.2.1}$$

$$D_{20}(S1,S3)=\frac{\overline{P}_0b^2}{32f_3}\left(\frac{f_3}{D}+1\right)-\frac{M^T}{4f_3},\quad D_{20}(S2,S4)=\frac{f_1M^T-f_2N^T+f_1f_4(\overline{P}_0b^2/8)}{4f_0}, \tag{A.2.2}$$

$$D_{10}(S1,S3)=-\frac{\overline{P}_0b^4}{64f_3}\left[\frac{f_3}{D}+2\right]-\frac{\overline{P}_0b^2}{4K^2A_2}+\frac{M^Tb^2}{4f_3},\quad D_{10}(S2,S4)=\frac{\overline{P}_0b^4}{64D}-\frac{\overline{P}_0b^2}{4K^2A_2}-b^2D_{20}, \tag{A.2.3}$$

where

$$f_0=f_2^2-f_1f_3,\quad f_1=A_1-A_2,\quad f_2=B_1-B_2,\quad f_3=D_1-D_2,\quad f_4=-(2+B_2\gamma-D2/D). \tag{A.2.4}$$

The remaining integration constants appearing in Eqs. (57.1, 2) are given as:

$$\tilde{A}_{11}(S1)=-\frac{g_1\mu^2\overline{P}_1b^4}{g_0},\quad \tilde{A}_{11}(S2,S3,S4)=-\frac{s_1\mu^2\overline{P}_1b^4}{s_0}, \tag{A.3.1}$$

$$\tilde{B}_{11}(S1)=\overline{P}_1b\frac{g_4[I_0(\mu b)+I_2(\mu b)]}{A_2g_0},\quad \tilde{B}_{11}(S2,S3,S4)=0, \tag{A.3.2}$$

$$\begin{aligned}
&D_{11}(S1)=\overline{P}_1b\frac{g_5[I_0(\mu b)+I_2(\mu b)]+g_6I_1(\mu b)}{16K^2A_2Dg_0},\\
&D_{11}(S2,S3,S4)=\overline{P}_1b\frac{s_4[I_0(\mu b)+I_2(\mu b)]+s_5I_1(\mu b)}{16K^2A_2Ds_0},\\
&D_{21}(S1)=\overline{P}_1b\frac{g_7[I_0(\mu b)+I_2(\mu b)]+g_8I_1(\mu b)}{8Dg_0},\\
&D_{21}(S2,S3,S4)=-\overline{P}_1b\frac{s_6[I_0(\mu b)+I_2(\mu b)]+s_7I_1(\mu b)}{8Ds_0},\\
&E_{11}(S1)=-\overline{P}_1b^3\frac{g_9[I_0(\mu b)+I_2(\mu b)]+g_{10}I_1(\mu b)}{16A_2Dg_0},\\
&E_{11}(S2)=\overline{P}_1b^3\frac{s_8[I_0(\mu b)+I_2(\mu b)]+s_9I_1(\mu b)}{16Ds_0},\\
&E_{11}(S3)=\overline{P}_1b^3\frac{s_{10}[I_0(\mu b)+I_2(\mu b)]+s_9I_1(\mu b)}{16Ds_0},\quad E_{11}(S4)=0,
\end{aligned} \tag{A.3.3}$$

where

$$
\begin{aligned}
&g_0 = 12[g_2(I_0(\mu b) + I_2(\mu b)) + g_3 I_1(\mu b)], \quad g_1 = g_{01}D_2 - 2A_2B_1^2/A_1,\\
&g_2 = \mu b\{-4g_{02} + e_{01}[2B_1^2 + g_{01}(-2D_1 + D_2)]\}, \quad g_3 = 8g_{02}, \quad g_4 = -b\mu e_{01}A_2B_1,\\
&g_5 = \begin{array}{c}\mu b\{96Dg_{02} + 16De_{01}[B_1(-3B_1 + B_2) + g_{01}(3D_1 - 2D_2)]\\ - e_{01}^2[g_{01}(-4D_1 + D_2) + 4B_1^2 + 2A_2(B_1^2/A_1)]\}\end{array}, \quad g_6 = -16g_{02}(12D + e_{01}),\\
&g_7 = \mu b\{-6g_{02} + e_{01}[g_{01}(-3D_1 + D_2) + (B_1^2/A_1)(3A_1 + A_2)]\}, \quad g_8 = 12g_{02},\\
&g_9 = \mu b\{-16B_2g_{02} + e_{01}A_2(B_1/A_1)[-10A_1D - 2D_1A_2 + D_2g_{01}]\},\\
&g_{10} = 16D[2B_1B_2^2 - A_2D_2(B_1 + B_2)], \quad g_{01} = A_1 + A_2, \quad g_{02} = D(2B_1B_2 - g_{01}D_2),\\
&s_0 = 12[s_2(I_0(\mu b) + I_2(\mu b)) + s_3 I_1(\mu b)], \quad s_1 = A_2(A_1D_2 - B_1B_2),\\
&s_2 = \mu b\{-4s_{01} + e_{01}A_2[B_1(2B_1 - B_2) + A_1(-2D_1 + D_2)]\}, \quad s_3 = 8s_{01},\\
&s_4 = \mu b\{96Ds_{01} - 16e_{01}DA_2[B_1(3B_1 - 2B_2) + A_1(-3D_1 + 2D_2)] + e_{01}^2A_2s_{02}\},\\
&s_5 = -16s_{01}(12D + e_{01}), \quad s_6 = \mu b\{6s_{01} + e_{01}A_2[B_1(B_2 - 3B_1) - A_1(D_2 - 3D_1)]\},\\
&s_7 = -12s_{01}, \quad s_8 = \mu b(B_1/A_1)(16s_{01} + A_2e_{01}s_{02}), \quad s_9 = -16(B_1/A_1)s_{01}.\\
&s_{10} = \mu b(B_1/A_1)\{16s_{01} + A_2e_{01}[B_1(B_2 - 8B_1) + A_1(8D_1 - D_2)]\},\\
&s_{01} = A_1D(B_2^2 - A_2D_2), \quad s_{02} = B_1(B_2 - 4B_1) + A_1(4D_1 - D_2)
\end{aligned}
\tag{A.3.4}
$$

with e_{01} being given in (A.1.5).

Appendix B

Upon substitution of Eq. (4) into (19.1, 2), the following results are obtained for the plate rigidities:

$$(A_1, B_1, D_1) = \frac{(A, B, \overline{D})}{1 - \upsilon^2} \quad \text{and} \quad (A_2, B_2, D_2) = \frac{(A, B, \overline{D})}{2(1 + \upsilon)}, \tag{B.1.1}$$

where

$$A = (E_m - E_c)\frac{h}{n+1} + E_c h, \quad B = -(E_m - E_c)\frac{h^2 n}{2(n+1)(n+2)} \tag{B.1.2}$$

and

$$\overline{D} = (E_m - E_c)\frac{h^3(n^2 + n + 2)}{4(n+1)(n+2)(n+3)} + E_c\frac{h^3}{12}. \tag{B.1.3}$$

References

[1] Koizumi, M.: The concept of FGM. Ceram. Trans. Funct. Gradient Mater. **34**, 3–10 (1993)

[2] Sureh, S., Mortensen, A.: Fundamentals of Functionally Graded Materials. IOM Communications Limited, London (1998)

[3] Durodola, J.F., Attia, O.: Deformation and stresses in functionally graded rotating disks. Comp. Sci. Technol. **60**, 987–995 (2000)

[4] Kawamura, R., Matsomoto, S., Tanigawa, Y.: Multipurpose optimization problem on material composition for thermal stress relaxation type of functionally graded circular plate using genetic algorithm. In: 3rd International Congress on Thermal Stresses (Thermal Stresses '99) (Skrzyspek, J.J., Hetnarski, R.B., eds.), pp. 479–482. Cracow (1999)

[5] Najafizadeh, M.M., Hedayati, B.: Refined theory for thermoelastic stability of functionally graded circular plates. J. Therm. Stress. **27**, 857–880 (2004)

[6] Najafizadeh, M.M., Heydari, H.R.: Thermal buckling of functionally graded circular plates based on higher order shear deformation plate theory. Eur. J. Mech. A/Solids **23**, 1085–1100 (2004)
[7] Najafizadeh, M.M., Eslami, M.R.: First-order-theory-based thermoelastic stability of functionally graded material circular plates. AIAA J. **40**, 1444–1450 (2002)
[8] Najafizadeh, M.M., Eslami, M.R.: Buckling analysis of circular plates of functionally graded materials under uniform radial compression. Int. J. Mech. Sci. **44**, 2479–2493 (2002)
[9] Cheng, Z.Q., Batra, R.C.: Three-dimensional thermoelastic deformations of a functionally graded elliptic plate. Composites Part B **31**, 97–106 (2000)
[10] Reddy, J.N., Wang, C.M., Kitipornchai, S.: Axisymmetric bending of functionally graded circular and annular plates. Eur. J. Mech. A/Solids **18**, 185–199 (1999)
[11] Ma, L.S., Wang, T.J.: Relationships between axisymmetric bending and buckling solutions of FGM circular plates based on third-order plate theory and classical plate theory. Int. J. Solids Struct. **41**, 85–101 (2004)
[12] Ma, L.S., Wang, T.J.: Nonlinear bending and post-buckling of a functionally graded circular plate under mechanical and thermal loadings. Int. J. Solids Struct. **40**, 3311–3330 (2003)
[13] Prakash, T., Ganapathi, M.: Asymmetric flexural vibration and thermoelastic stability of FGM circular plates using finite element method. Composites Part B **37**, 642–649 (2006)
[14] Mindlin, R.D.: Influence of rotatory inertia and shear on flexural motions of isotropic, elastic plates. J. Appl. Mech. **18**, 31–38 (1951)
[15] Reissner, E.: The effect of transverse shear deformation on the bending of elastic plates. J. Appl. Mech. **12**, 69–77 (1945)
[16] Reissner, E.: On bending of elastic plates. Q. Appl. Math. **5**, 55–68 (1947)
[17] Nosier, A., Reddy, J.N.: A study of non-linear dynamics equation of higher order shear deformation plate theories. Int. J. Nonlinear Mech. **22**, 233–249 (1991)
[18] Nosier, A., Reddy, J.N.: On boundary layer and interior equations for higher order theories of plates. J. Appl. Math. Mech. (ZAMM) **72**, 657–666 (1992)
[19] Nosier, A., Reddy, J.N.: On vibration and buckling of symmetric laminated plates according to shear deformation theories. Part I. Acta Mech. **94**, 123–144 (1992)
[20] Nosier, A., Reddy, J.N.: On vibration and buckling of symmetric laminated plates according to shear deformation theories. Part II. Acta Mech. **94**, 145–169 (1992)
[21] Nosier, A., Yavari, A., Sarkani, S.: Study of edge-zone equation of Mindlin–Reissner plate theory. J. Engng. Mech. **126**, 647–651 (2000)
[22] Nosier, A., Yavari, A., Sarkani, S.: On a boundary layer phenomenon in Mindlin-Reissner plate theory for laminated circular sector plates. Acta Mech. **151**, 149–161 (2001)
[23] Reddy, J.N.: A simple higher-order theory for laminated composite plates. J. Appl. Mech. **51**, 745–752 (1984)
[24] Reddy, J.N., Chin, C.D.: Thermo-mechanical analysis of functionally graded cylinders and plates. J. Therm. Stress. **21**, 593–626 (1998)
[25] Tuma, J.J.: Engineering Mathematics Handbook, Definitions, Theorems, Formulas, Tables. McGraw-Hill, New York (1970)
[26] Fung, Y.C., Tong, P.: Classical and Computational Solid Mechanics. World Scientific, New Jersey (2001)
[27] Reddy, J.N.: Theory and Analysis of Elastic Plates. Taylor& Francis, Philadelphia (1999)
[28] Irschik, H.: On vibrations of layered beams and plates. J. Appl. Math. Mech. (ZAMM) **73**, T34–T45 (1993)
[29] Hildebrand, F.B.: Advanced Calculus for Applications. Prentice-Hall, New Jersey (1962)